

Concentration, Spin and Shape of Dark Matter Haloes as a Function of the Cosmological Model: WMAP1, WMAP3 & WMAP5 results.

Andrea V. Macciò¹*, Aaron A. Dutton², Frank C. van den Bosch¹

¹*Max-Planck-Institut für Astronomie, Königstuhl 17, 69117 Heidelberg, Germany*

²*UCO/Lick Observatory and Department of Astronomy and Astrophysics, University of California, Santa Cruz, CA*

ABSTRACT

We investigate the effects of changes in the cosmological parameters between the WMAP 1st, 3rd, and 5th year results on the structure of dark matter haloes. We use a set of simulations that cover 5 decades in halo mass ranging from the scales of dwarf galaxies ($V_c \approx 30$ km/s) to clusters of galaxies ($V_c \approx 1000$ km/s). We find that the concentration mass relation is a power law in all three cosmologies. However the slope is shallower and the zero point is lower moving from WMAP1 to WMAP5 to WMAP3. For haloes of mass $\log M_{200}/[h^{-1} M_\odot] = 10, 12,$ and 14 the differences in the concentration parameter between WMAP1 and WMAP3 are a factor of 1.55, 1.41, and 1.29, respectively. As we show, this brings the central densities of dark matter haloes in good agreement with the central densities of dwarf and low surface brightness galaxies inferred from their rotation curves, for both the WMAP3 and WMAP5 cosmologies. We also show that none of the existing toy models for the concentration-mass relation can reproduce our simulation results over the entire range of masses probed. In particular, the model of Bullock et al. (2001a; hereafter B01) fails at the higher mass end ($M \gtrsim 10^{13} h^{-1} M_\odot$), while the NFW model of Navarro, Frenk & White (1997) fails dramatically at the low mass end ($M \lesssim 10^{12} h^{-1} M_\odot$). We present a new model, based on a simple modification of that of B01, which reproduces the concentration-mass relations in our simulations over the entire range of masses probed ($10^{10} h^{-1} M_\odot \lesssim M \lesssim 10^{15} h^{-1} M_\odot$). Haloes in the WMAP3 cosmology (at a fixed mass) are more flatted compared to the WMAP1 cosmology, with a medium to long axis ratio reduced by $\approx 10\%$. Finally, we show that the distribution of halo spin parameters is the same for all three cosmologies.

Key words: galaxies: haloes – cosmology:theory, dark matter, gravitation – methods: numerical, N-body simulation

1 INTRODUCTION

In the paradigm of hierarchical structure formation, dark matter (DM) haloes provide the potential well in which galaxies subsequently form. As a consequence the structural parameters of disk galaxies (size and rotation velocity) are tightly coupled with those of their hosting DM halo, such as concentration and spin (e.g. Mo, Mao & White 1998; Dutton et al. 2007).

It has been shown by several studies that the structural properties of dark matter haloes are dependent on halo mass: for example higher mass haloes are less concen-

trated (Navarro, Frank & White 1997, hereafter NFW; Bullock et al. 2001a, hereafter B01; Eke Navarro & Steinmetz 2001; Kuhlen et al. 2005; Neto et al. 2007; Macciò et al. 2007, hereafter M07), and are more prolate (Jing & Suto 2002; Allgood et al. 2006; M07) on average. In the case of the spin parameter, however, there seems to be no mass dependence.

In M07 we used a set of numerical simulations of structure formation in a Λ CDM cosmology, with cosmological parameters that were motivated by the first year results of the Wilkinson Microwave Anisotropy Probe (WMAP) mission (Spergel et al. 2003; hereafter WMAP1), to study how concentrations, shapes and spin parameters of dark matter haloes scale with halo mass. In this paper we extend the M07 study by investigating how these scaling relations de-

* maccio@mpia.de

Table 1. Cosmological Parameters

Name	$\Omega_\Lambda + \Omega_m$	Ω_m	h	σ_8	n	Ω_b
WMAP1	1.0	0.268	0.71	0.90	1.00	0.044
WMAP3	1.0	0.238	0.73	0.75	0.95	0.042
WMAP5	1.0	0.258	0.72	0.796	0.963	0.0438

pend on the adopted cosmology. In particular, we present a large suite of numerical simulations for Λ CDM cosmologies whose parameters are motivated by the three and five year data releases of the WMAP mission (Spergel et al. 2007; Komatsu et al. 2008). In what follows we refer to these cosmologies as the WMAP3 and WMAP5 cosmologies, respectively. The parameters of the WMAP1, WMAP3 and WMAP5 cosmologies are listed in Table 1. Note that the WMAP3 and WMAP5 cosmologies both have a lower matter density, Ω_m , and a lower power spectrum normalization, σ_8 (defined as the rms of the matter field, linearly extrapolated to the present, on a scale of $8h^{-1}$ Mpc) than the WMAP1 cosmology. This implies that dark matter haloes of a given mass assemble later (e.g., van den Bosch 2001). Since the concentration of a dark matter halo is related to its assembly redshift (e.g., Wechsler et al. 2002; Zhao et al. 2003a,b; Li et al. 2007), dark matter haloes are expected to be less concentrated in the WMAP3 and WMAP5 cosmologies. This may help to reconcile the conflict between the concentration parameters inferred from the rotation curves of dwarf and low surface brightness (LSB) galaxies (de Blok, McGaugh & Rubin 2001; Swaters et al. 2003) and those predicted from the Λ CDM scenario. In addition, a lower amplitude of the power spectrum results in haloes being more prolate (Allgood et al. 2006), which may have observational implications for the rotation curves of dark matter dominated galaxies.

As in M07 we use a large suite of N-body simulations for the WMAP1, WMAP3 and WMAP5 cosmologies with different box sizes to cover the entire halo mass range from $10^{10}h^{-1}M_\odot$ (haloes that host dwarf galaxies) to $10^{15}h^{-1}M_\odot$ (massive clusters). We use these simulations to investigate the concentrations, spin parameters of shapes of dark matter haloes. We also present a critical comparison of the simulation results with two toy models for the concentration-mass relation. In particular, we show that the B01 model is only able to reproduce the simulation results in the galaxy mass range, but underpredicts the concentrations of massive haloes. On the contrary, the NFW model yields a reasonable fit at the massive end, but dramatically underestimates the concentrations for haloes with $M \lesssim 10^{12}h^{-1}M_\odot$. We present a new model, based on a simple modification of the B01 model, that is able to reproduce the concentration-mass relation over the entire mass range probed by our numerical simulations.

This paper is organized as follows: in Section 2 the simulations and the determination of the halo parameters are presented. In Sections 3, 4 and 5 we discuss the results for halo concentrations, spins and shapes respectively. Finally, Section 6 summarizes the results.

Table 2. N-body Simulation Parameters

Name	Box size [Mpc]	N	part. mass [$h^{-1}M_\odot$]	force soft. [h^{-1} kpc]	Nhalo > 500
W1-20.1	20	250 ³	1.36e7	0.43	814
W1-20.2	20	250 ³	1.36e7	0.43	849
W1-40.1	40	250 ³	1.09e8	0.85	1132
W1-40.2	40	250 ³	1.09e8	0.85	1018
W1-90.1	90	300 ³	7.19e8	1.92	2552
W1-90.2	90	300 ³	7.19e8	1.92	1992
W1-90.3	90	600 ³	8.98e7	0.85	12766
W1-180	180	300 ³	5.75e9	3.83	2406
W1-300	300	400 ³	1.12e10	4.72	6415
W3-20.1	20	250 ³	1.32e7	0.43	960
W3-20.2	20	250 ³	1.32e7	0.43	1011
W3-40.1	40	250 ³	1.05e8	0.85	1108
W3-90.1	90	300 ³	6.94e8	1.92	1963
W3-90.2	90	300 ³	6.94e8	1.92	2043
W3-90.3	90	600 ³	8.67e7	0.85	13143
W3-180	180	300 ³	5.55e9	3.83	2105
W3-300	300	400 ³	1.08e10	4.78	5255
W3-360	360	400 ³	1.87e10	5.74	4947
W3-360.2	360	600 ³	5.55e9	3.83	17582
W5-20.1	20	250 ³	1.37e7	0.43	974
W5-40.1	40	250 ³	1.09e8	0.85	1119
W5-90.1	90	300 ³	7.21e8	1.92	1998
W5-180	180	300 ³	5.77e9	3.83	2302
W5-300	300	400 ³	1.13e10	4.74	5845

2 N-BODY SIMULATIONS

Table 2 lists all the simulations used in this paper. Each simulation has a unique name, Wx -LL. n , where $x = 1, 3, 5$ refers to the WMAP1, WMAP3 and WMAP5 cosmology, respectively, LL is the simulation box size in Mpc, and n is a sequential integer. For each cosmology we have run simulations for five different box sizes, which allows us to probe halo masses covering the entire range $10^{10}h^{-1}M_\odot \lesssim M \lesssim 10^{15}h^{-1}M_\odot$. In addition, in some case we have run multiple (up to three) simulations for the same cosmology and box size, in order to test for the impact of cosmic variance (and to increase the final number of dark matter haloes).

All simulations have been performed with PKDGRAV, a tree code written by Joachim Stadel and Thomas Quinn (Stadel 2001). The code uses spline kernel softening, for which the forces become completely Newtonian at 2 softening lengths. Individual time steps for each particle are chosen proportional to the square root of the softening length, ϵ , over the acceleration, a : $\Delta t_i = \eta \sqrt{\epsilon/a_i}$. Throughout, we set $\eta = 0.2$, and we keep the value of the softening length constant in co-moving coordinates during each run. The physical values of ϵ at $z = 0$ are listed in Table 2. Forces are computed using terms up to hexadecapole order and a node-opening angle θ which we change from 0.55 initially to 0.7 at $z = 2$. This allows a higher force accuracy when the mass distribution is nearly smooth and the relative force errors can be large. The initial conditions are generated with the GRAFIC2 package (Bertschinger 2001). The starting redshifts z_i are set to the time when the standard deviation

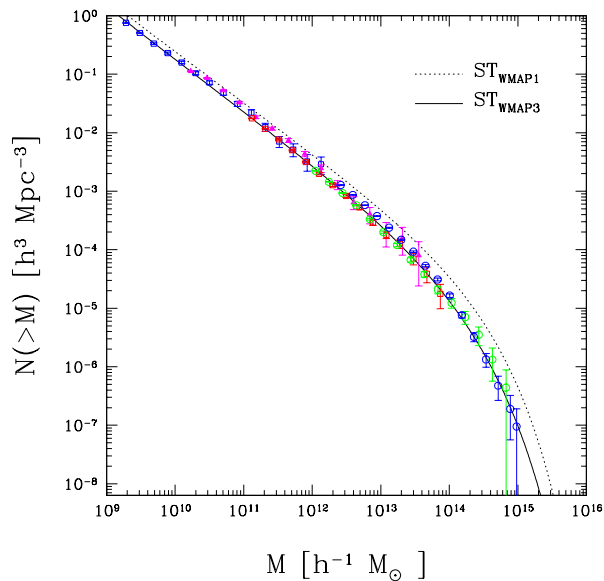


Figure 1. Mass functions for the WMAP3 simulations (only one simulation per box size is shown). The dotted and solid lines represents the Sheth & Tormen (2001) prediction for the WMAP1 and WMAP3 models respectively. Error bars indicate the Poisson noise in each mass bin.

of the smallest density fluctuations resolved within the simulation box reaches 0.2 (the smallest scale resolved within the initial conditions is defined as twice the intra-particle distance).

In all simulations, dark matter haloes are identified using a spherical overdensity (SO) algorithm. Candidate groups with a minimum of $N_f = 250$ particles are selected using a FoF algorithm with linking length $\phi = 0.2 \times d$ (the average particle separation). We then: (i) find the point C where the gravitational potential is minimum; (ii) determine the radius \bar{r} of a sphere centered on C , where the density contrast is Δ , with respect to the *critical density* of the Universe, $\rho_{\text{crit}} = 3H^2/8\pi G$. Using all particles in the corresponding sphere we iterate the above procedure until we converge onto a stable particle set. For each stable particle set we obtain the virial radius, r_{vir} , the number of particles within the virial radius, N_{vir} , and the virial mass, M_{vir} . For our adopted cosmologies $\Delta \simeq 96.7$ (WMAP1), $\Delta \simeq 93.5$ (WMAP3) and $\Delta \simeq 95.1$ (WMAP5). These values are based on the fitting function of Mainini et al. (2003).

Throughout this paper we only use haloes with $N_{\text{vir}} > 500$, of which we there are 29944, 50177, and 12238 in the combined WMAP1, WMAP3 and WMAP5 simulations, respectively. For completeness, Fig. 1 shows the halo mass function obtained from the WMAP3 simulations, together with the predictions from Sheth & Tormen (2001) for the WMAP1 and WMAP3 cosmologies (error bars show the Poisson noise in each mass bin). Note that the mass function obtained from our simulation is in excellent agreement with this prediction and that the WMAP3 cosmology predicts fewer haloes per co-moving volume than the WMAP1 cosmology, especially at the massive end.

2.1 Halo parameters

For each SO halo in our sample we determine a set of parameters, including the virial mass and radius, the concentration parameter, the angular momentum, the spin parameter and various axis ratios (shape). Below we briefly describe how these parameters are defined and determined. A more detailed discussion can be found in M07.

2.1.1 Concentration parameter

To compute the concentration of a halo we first determine its density profile. The halo center is defined as the location of the most bound halo particle, and we compute the density (ρ_i) in 50 spherical shells, spaced equally in logarithmic radius. Errors on the density are computed from the Poisson noise due to the finite number of particles in each mass shell. The resulting density profile is fit with a NFW profile (Navarro et al. 1997):

$$\frac{\rho(r)}{\rho_{\text{crit}}} = \frac{\delta_c}{(r/r_s)(1+r/r_s)^2}, \quad (1)$$

During the fitting procedure we treat both r_s and δ_c as free parameters. Their values, and associated uncertainties, are obtained via a χ^2 minimization procedure using the Levenberg & Marquart method. We define the r.m.s. of the fit as:

$$\rho_{\text{rms}} = \frac{1}{N} \sum_i^N (\ln \rho_i - \ln \rho_m)^2 \quad (2)$$

where ρ_m is the fitted NFW density distribution. Finally, we define the concentration of the halo, $c_{\text{vir}} \equiv r_{\text{vir}}/r_s$, using the virial radius obtained from the SO algorithm, and we define the error on $\log c$ as $(\sigma_{r_s}/r_s)/\ln(10)$, where σ_{r_s} is the fitting uncertainty on r_s . In order to compare our results with previous studies it is also useful to define, $c_{200} \equiv r_{200}/r_s$, where r_{200} is the radius inside of which the density of the dark matter halo is 200 times ρ_{crit} ; accordingly we also define M_{200} and N_{200} as the mass and the number of particles within r_{200} .

2.1.2 Spin parameter

The spin parameter is a dimensionless measure of the amount of rotation of a dark matter halo. We use the definition introduced by Bullock et al. (2001b):

$$\lambda = \frac{J_{\text{vir}}}{\sqrt{2}M_{\text{vir}}V_{\text{vir}}r_{\text{vir}}} \quad (3)$$

where M_{vir} , J_{vir} and V_{vir} are the mass, total angular momentum and circular velocity at the virial radius, respectively. See M07 for a detailed discussion and for a comparison of the different definitions for the spin parameter.

2.1.3 Shape parameter

Determining the shape of a three-dimensional distribution of particles is a non-trivial task (e.g., Jing & Suto 2002). Following Allgood et al. (2006) we determine the shapes of our haloes starting from the inertia tensor. As a first step, we compute the halo's 3×3 inertia tensor using all the particles within the virial radius. Next we diagonalize the inertia

tensor and rotate the particle distribution according to the eigen vectors. In this new frame (in which the moment of inertia tensor is diagonal) the ratios $s = a_3/a_1$ and $p = a_3/a_2$ (where $a_1 \geq a_2 \geq a_3$) are given by:

$$s \equiv \frac{a_3}{a_1} = \sqrt{\frac{\sum m_i z_i^2}{\sum m_i x_i^2}}, \quad p \equiv \frac{a_3}{a_2} = \sqrt{\frac{\sum m_i z_i^2}{\sum m_i y_i^2}}. \quad (4)$$

Next we again compute the inertia tensor, but this time only using the particles inside the ellipsoid defined by a_1 , a_2 and a_3 . When deforming the ellipsoidal volume of the halo, we keep the longest axis (a_1) equal to the original radius of the spherical volume (r_{vir}). We iterate this procedure until we converge to a stable set of axis ratios.

2.1.4 Offset parameter

As in M07, for each halo we compute the offset parameter, x_{off} , defined as the distance between the most bound particle (used as the center for the density profile) and the center of mass of the halo, in units of the virial radius. This offset is a measure of the dynamical state of the halo: relaxed haloes in equilibrium will have a smooth, radially symmetric density distribution, and thus an offset parameter that is virtually equal to zero. Unrelaxed haloes, such as those that have only recently experienced a major merger, are likely to have a strongly asymmetric mass distribution, and thus a relatively large x_{off} . Although some unrelaxed haloes may have a small x_{off} , the advantage of this parameter over, for example, the actual virial ratio, $2T/V$, as a function of radius (Macciò, Murante & Bonometto 2003; Shaw et al. 2006), is that the former is trivial to evaluate.

2.2 Relaxed Haloes

Our halo finder (and halo finders in general) does not distinguish between relaxed and unrelaxed haloes. There are many reasons why we might want to remove unrelaxed haloes. First and foremost, unrelaxed haloes often have poorly defined centers, which makes the determination of a radial density profile, and hence of the concentration parameter, an ill-defined problem. Moreover unrelaxed haloes often have shapes that are not adequately described by an ellipsoid, making our shape parameters ill-defined as well.

One could imagine using ρ_{rms} (the r.m.s. of the NFW fit to the density profile) to decide whether a halo is relaxed or not. However, while it is true that ρ_{rms} is typically high for unrelaxed haloes, haloes with relatively few particles also have a high ρ_{rms} (due to Poisson noise) even when they are relaxed (cf. Fig.2 of M07 for the correlation between ρ_{rms} and N_{vir}). Furthermore, since the spherical averaging used to compute the density profiles has a smoothing effect, not all unrelaxed haloes have a high ρ_{rms} . However, these haloes are often characterized by a large offset parameter, x_{off} . We therefore use both ρ_{rms} and x_{off} to judge whether a halo is relaxed or not. Following M07 we split our halo sample in unrelaxed and relaxed haloes. The latter are defined as the haloes with $\rho_{\text{rms}} < 0.5$ and $x_{\text{off}} < 0.07$. About 70% of the haloes in our sample qualify as relaxed haloes. In what follow, we will present results for two different samples of haloes: ALL, which includes all haloes with $N_{\text{vir}} > 500$,

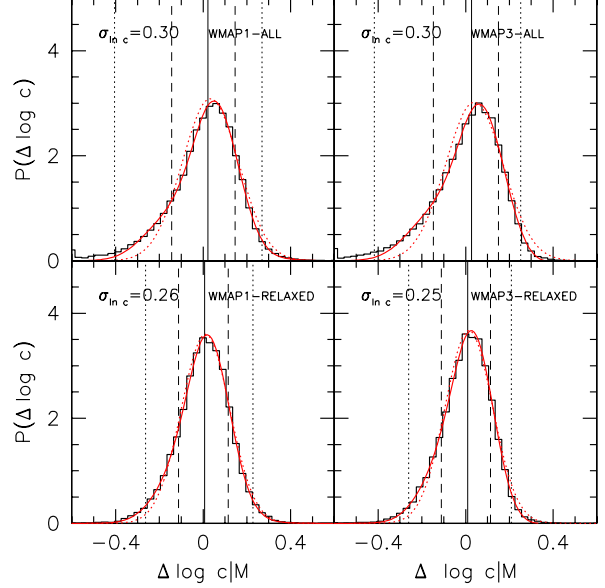


Figure 4. Histograms of residuals from the mean c_{200} mass relations in Fig. 3. Only results for WMAP1 and WMAP3 are shown; results for WMAP5 are listed in Table A2. The vertical lines show the 2.3th, 13.9th, 50th, 84.1th, and 97.7th percentiles of the concentration residuals. The solid red line shows a Gauss-Hermite polynomial expansion up to fourth order (whose parameters are given in Table A2), the dashed red line shows the Gaussian corresponding to the zeroth order of this expansion. The logarithmic variance ($\sigma_{\text{in } c}$) of the Gaussian fit is reported in the top left corner of each panel.

and RELAXED, which is the corresponding subsample of relaxed haloes.

3 CONCENTRATION-MASS RELATION

3.1 Differences between WMAP1, WMAP3 and WMAP5

We first discuss the concentration-mass (hereafter c - M) relation. Figs. 2 and 3 show the $c_{\text{vir}} - M_{\text{vir}}$ and $c_{200} - M_{200}$ relations for the WMAP1, WMAP3 and WMAP5 cosmologies, and for both the ALL and RELAXED samples, as indicated. The symbols show the mean concentrations (in logarithmic space) in mass bins of 0.4 dex width. For all three cosmologies the c - M relation is well fit by a single power-law (red solid line). For the relaxed haloes, these best-fit power-laws relations are given by

$$\log c_{\text{vir}} = 1.051 - 0.099 \log(M_{\text{vir}}/[10^{12} h^{-1} M_{\odot}]) \quad (5)$$

$$\log c_{200} = 0.917 - 0.104 \log(M_{200}/[10^{12} h^{-1} M_{\odot}]) \quad (6)$$

for the WMAP1 cosmology, and

$$\log c_{\text{vir}} = 0.915 - 0.080 \log(M_{\text{vir}}/[10^{12} h^{-1} M_{\odot}]) \quad (7)$$

$$\log c_{200} = 0.769 - 0.083 \log(M_{200}/[10^{12} h^{-1} M_{\odot}]) \quad (8)$$

for the WMAP3 cosmology, and

$$\log c_{\text{vir}} = 0.971 - 0.094 \log(M_{\text{vir}}/[10^{12} h^{-1} M_{\odot}]) \quad (9)$$

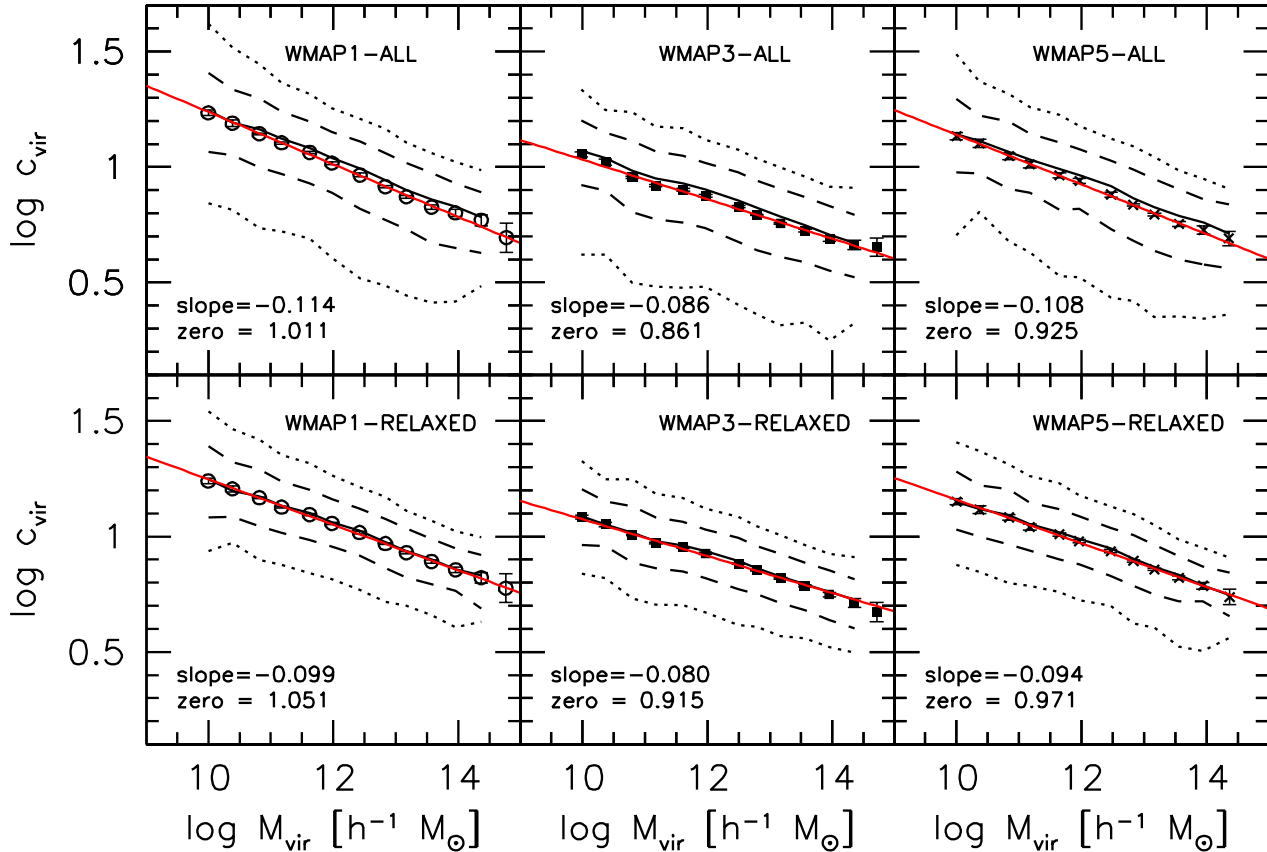


Figure 2. c_{vir} vs M_{vir} for WMAP1 (left), WMAP3 (center) and WMAP5 (right). The upper panels show all haloes with more than 500 particles within r_{vir} , while the lower panels show the “relaxed” haloes. The points show the mean concentration (in $\log c_{\text{vir}}$) in bins of width 0.4 dex in mass, the error bar shows the Poisson error on the mean. The solid lines represent the median concentration in each mass bin, the dashed and dotted lines show the 15.9, 84.1, 2.3 and 97.7th percentiles of the distribution. The solid (red) line shows a power-law fit to the $c_{\text{vir}} - M_{\text{vir}}$ relation: $\log c_{\text{vir}} = \text{zero} + \text{slope}(\log M_{\text{vir}}/12h^{-1}M_{\odot})$ whose parameters are given in the lower left corner of each panel, and in Table A1.

$$\log c_{200} = 0.830 - 0.098 \log(M_{200}/[10^{12}h^{-1}M_{\odot}]) \quad (10)$$

for the WMAP5 cosmology. The errors of these fitting parameters are listed in Table A1. Note that these relations differ in both the slope and the zero-point. In particular, going from WMAP1 to WMAP5 to WMAP3, the slopes become shallower and the zero-points become smaller. Comparing the WMAP1 and WMAP3 cosmologies, which are the extremes in terms of the cosmological parameter values (see Table 1), the difference in the mean $\log c_{\text{vir}}$ is 0.19, 0.15, 0.11 dex (i.e., a factor of 1.55, 1.41, 1.29 in c_{vir}) at a halo mass of 10^{10} , 10^{12} , $10^{14}h^{-1}M_{\odot}$. A similar trend of lower normalization and shallower slopes is also seen going towards higher redshift for a given cosmology (e.g. Zhao et al. 2003a). This supports the notion that the c - M relation reflects the assembly histories of dark matter haloes: the fact that WMAP3 haloes are less concentrated than their counterparts in a WMAP1 (or WMAP5) cosmology, simply reflects that haloes assemble later in a universe with lower Ω_m and/or lower σ_8 . Note that the three cosmologies also differ in the spectral index of the matter power spectrum, n , which is also responsible for some of the differences in the c - M relations.

Fig. 4 shows the distributions of the concentration residuals, $\Delta \log c_{200}$, relative to the best-fit power-laws $c_{200}(M_{200})$, for the WMAP1 and WMAP3 cosmologies. The full set of haloes (upper panels) shows a clear skewness towards low concentrations. This was already pointed out by M07, and is even apparent in the simulations of B01. As discussed by M07, this tail of low concentration parameters is due to unrelaxed haloes. Removing these haloes results in almost Gaussian distributions in $\Delta \log c_{200}$, as is apparent from the lower panels in Fig. 4. Table A2 lists a number of parameters for these distributions, including those for the WMAP5 cosmology (not shown in Fig. 4). Note that the scatter these distributions is virtually the same for all three cosmologies; hence, although the slope and zero-point of the c - M relation is clearly cosmology dependent, the scatter is not.

3.2 Comparison of WMAP1 results with the Millennium Simulation

Recently, Neto et al. (2007) analysed the c - M relation of dark matter haloes in the Millennium simulation (Springel et al. 2005). They confirm many of the results published previously in M07, namely:

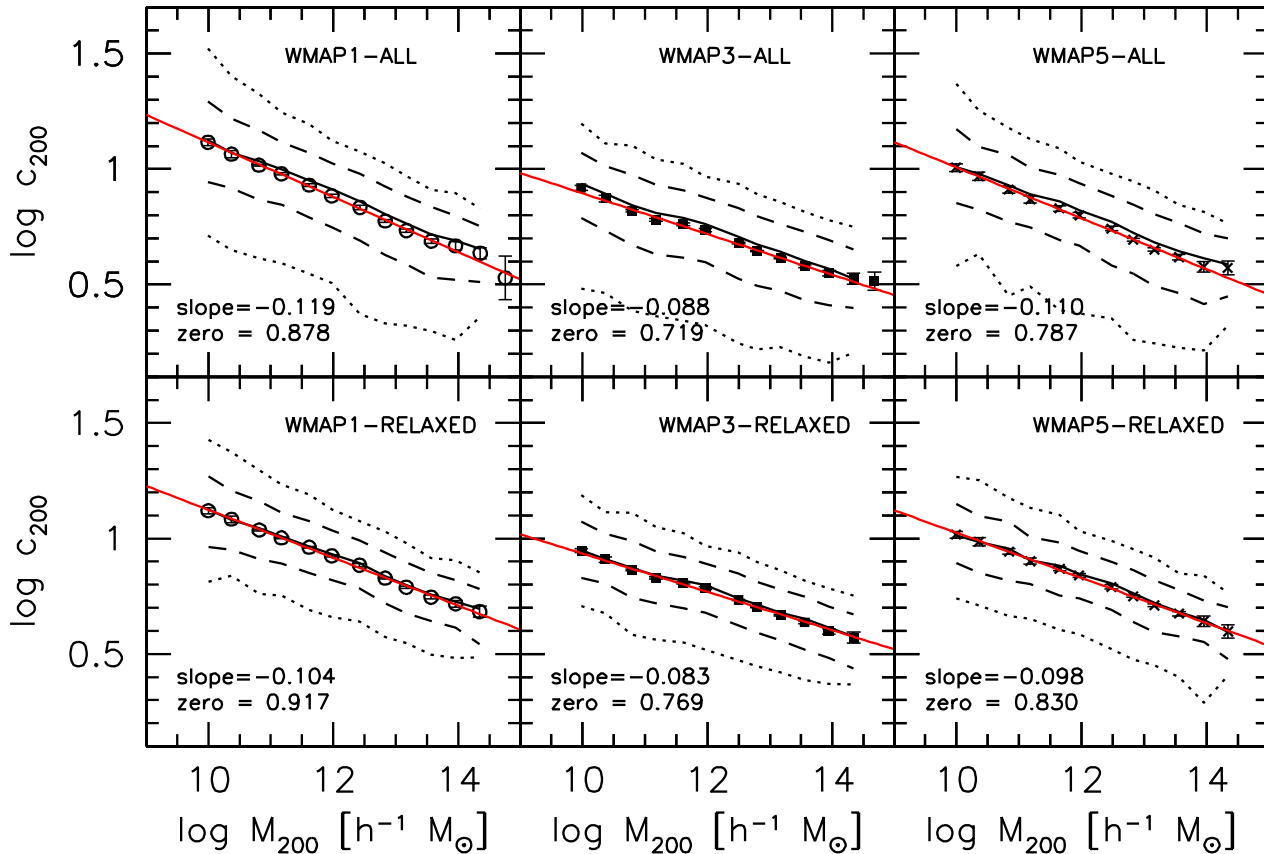


Figure 3. Same as Figure 2, but for c_{200} as function of M_{200} .

(i) The concentration mass relation (at redshift zero) is well described by a single power-law with slope $\simeq -0.10$.

(ii) The inclusion of un-relaxed haloes biases the zero-point low, and increases the scatter.

(iii) The inclusion of un-relaxed haloes is largely responsible for creating a false correlation between concentration parameter and spin parameter.

The symbols in Fig. 5 show the same mean $\log c_{200}$ as function of M_{200} as shown in Fig. 3. The solid red lines in the left-hand panels indicate the best-fit relation obtained by Neto et al. (2007) from the Millennium simulation¹. For both the full sample of haloes and for the subsamples of relaxed haloes, the Neto et al. (2007) results are in excellent agreement with our simulation data over the range of haloes probed our simulations. Note that, for comparison, the Millennium simulation only covered the range $10^{12} h^{-1} M_{\odot} \lesssim M_{200} \lesssim 10^{15} h^{-1} M_{\odot}$. This agreement is extremely encouraging because the Millennium simulation was run with a different N -body code (GADGET, rather than

PKDGRAV), and Neto et al. (2007) used a different halo finder.

Yet, Neto et al. (2007) questioned the results of M07 at small masses. They argued that at least 1000 particles are needed to reliably determine halo concentrations, and they conjecture that the small box size (20 Mpc) of the highest resolution simulation in M07 will be biased by missing large scale power. They conclude that some of the differences found in M07 between the Eke et al. (2001) model and their simulation results at small scales (at a few $10^{10} h^{-1} M_{\odot}$) are unreliable. Note, however, that the differences between the Eke et al. (2001) model and the M07 simulations are statistically significant, even at $10^{11} h^{-1} M_{\odot}$ (i.e on scales resolved with more than 1000 particles). Furthermore, the speculation by Neto et al. (2007) that the 20 Mpc boxes give biased halo concentrations is not justified: as was clearly shown in M07, the scatter in the c - M relation is independent of the large scale environment. To further bolster the results of M07 at masses below $1 \times 10^{11} h^{-1} M_{\odot}$, in this paper we include new simulations of 90 Mpc boxes with 216 million particles. These simulations have a particle mass of $9 \times 10^7 h^{-1} M_{\odot}$, which is an order of magnitude higher than that of the Millennium simulation.

¹ Note that the cosmology adopted for the Millennium simulation is very close, but not exactly the same as for our WMAP1 cosmology. For the purpose of our discussion, though, these differences are completely negligible.

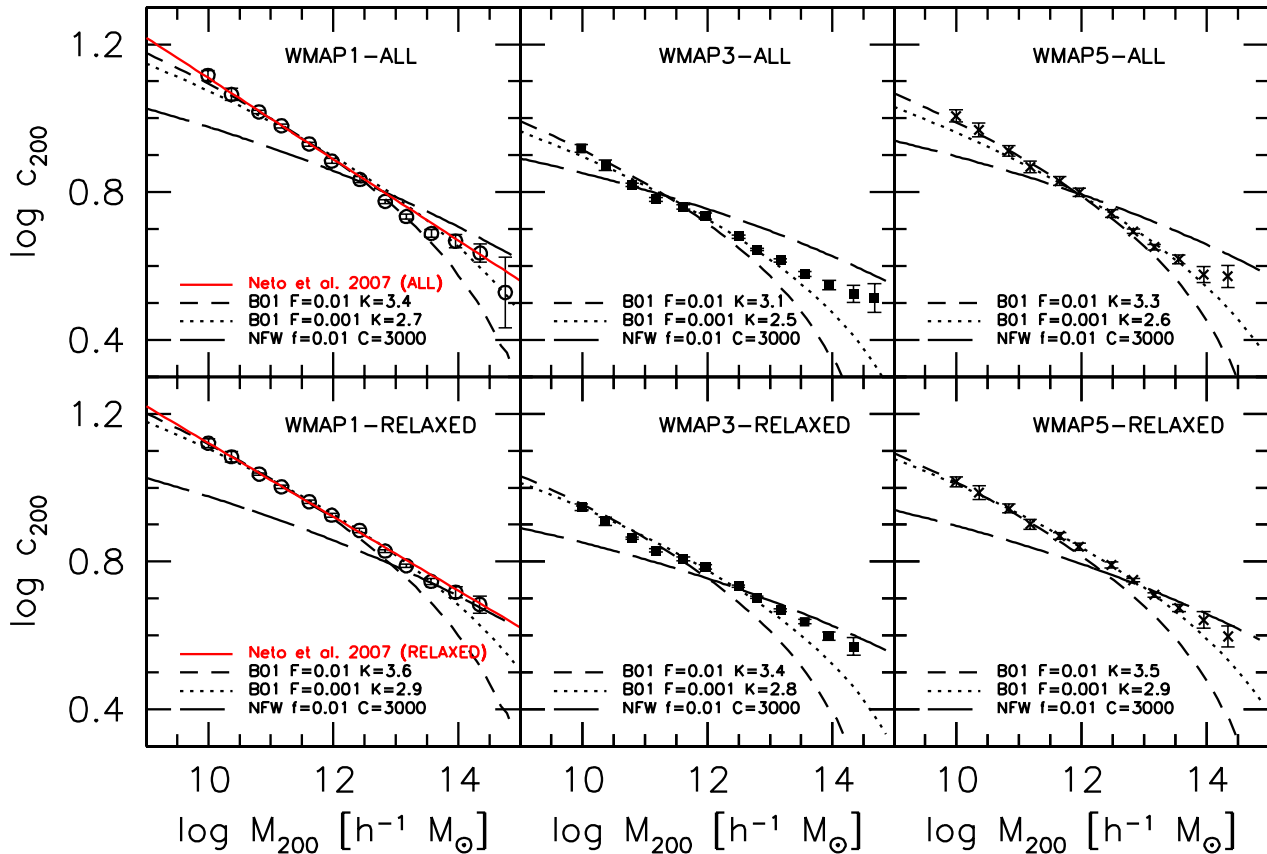


Figure 5. Comparison between the $c_{200} - M_{200}$ relations in our simulations and those predicted by the toy models of Bullock et al. (2001a, dotted and dashed lines) and NFW (1997) (long-dashed lines). For the Bullock et al. models we show the value of K that results in the best fit for galaxy mass haloes, for the NFW model we use the same value of C for all models. The solid (red) line shows the concentration-mass relations from the Millennium simulations as measured by Neto et al. (2007). See text for further details.

3.3 Comparison with toy models

A number of studies have presented analytical models for the $c-M$ relation, that have been calibrated against numerical simulations, but only over a relatively narrow range in halo mass. Here we compare our simulation results, which cover 5 orders of magnitude in halo mass, to two of the most commonly used models: that by Bullock et al. (2001a; hereafter the B01 model), and that by Navarro et al. (1997; hereafter the NFW model). Both these models have 2 free parameters (F and K for B01, f and C for NFW) that have been tuned to reproduce some simulation results. Fig. 5 shows the predictions for the $c - M$ relation for these models. B01 advocated a model with $F = 0.01$ and $K = 4.0$ which fit the $c - M$ relation of galaxy sized DM haloes ($10^{11} - 10^{13} h^{-1} M_{\odot}$). These parameters were obtained for a flat Λ CDM cosmology with $\Omega_m = 0.3$ and $\sigma_8 = 1.0$. A slightly lower normalization, $K = 3.4$, was advocated by M07 for a WMAP1 cosmology (see Zhao et al. 2003a and Kuhlen et al. 2005 for more details).

This $K = 3.4, F = 0.01$ model is shown as the long dashed line in the upper left-hand panel (ALL sample) of Figure 5. It fits the data from $M = 10^{10} h^{-1} M_{\odot}$ to $M = 10^{13} h^{-1} M_{\odot}$, but under-predicts the $c - M$ relation at high

masses. Neto et al. (2007) argue that this is a fundamental failure of the B01 model. However, as stressed by B01 (in both their paper and in their publicly available source code), their model is not expected to work on scales where $F \times M_{\text{vir}} \gtrsim M_*$. A partial solution is to adopt a lower value for F ; for instance using $F = 0.001$ and $K = 2.7$ yields a good fit to our simulation data over the range $10^{11} h^{-1} M_{\odot} \lesssim M \lesssim 10^{14} h^{-1} M_{\odot}$ (dotted line).

By contrast, the NFW model is in reasonable agreement with the $c-M$ relation of relaxed haloes at the high mass end. This model, with parameters advocated in the original paper by Navarro et al. (1997) ($f = 0.01, C = 3000$), is given by the long-dashed lines. This model matches the slope of the $c - M$ relation for the highest masses $M > 10^{13} h^{-1} M_{\odot}$. However, it dramatically underpredicts the concentrations of low mass haloes; in fact, the NFW model predict a slope for the $c-M$ relation which is much shallower than what we infer from our simulations, causing the discrepancy to increase with decreasing halo mass. Neto et al. (2007) gloss over these differences by saying that the differences are small compared to the scatter in c , i.e. since the scatter in c is a factor of 1.4, the discrepancy between the NFW model and the simulation results is less than 1σ . However, the relevant

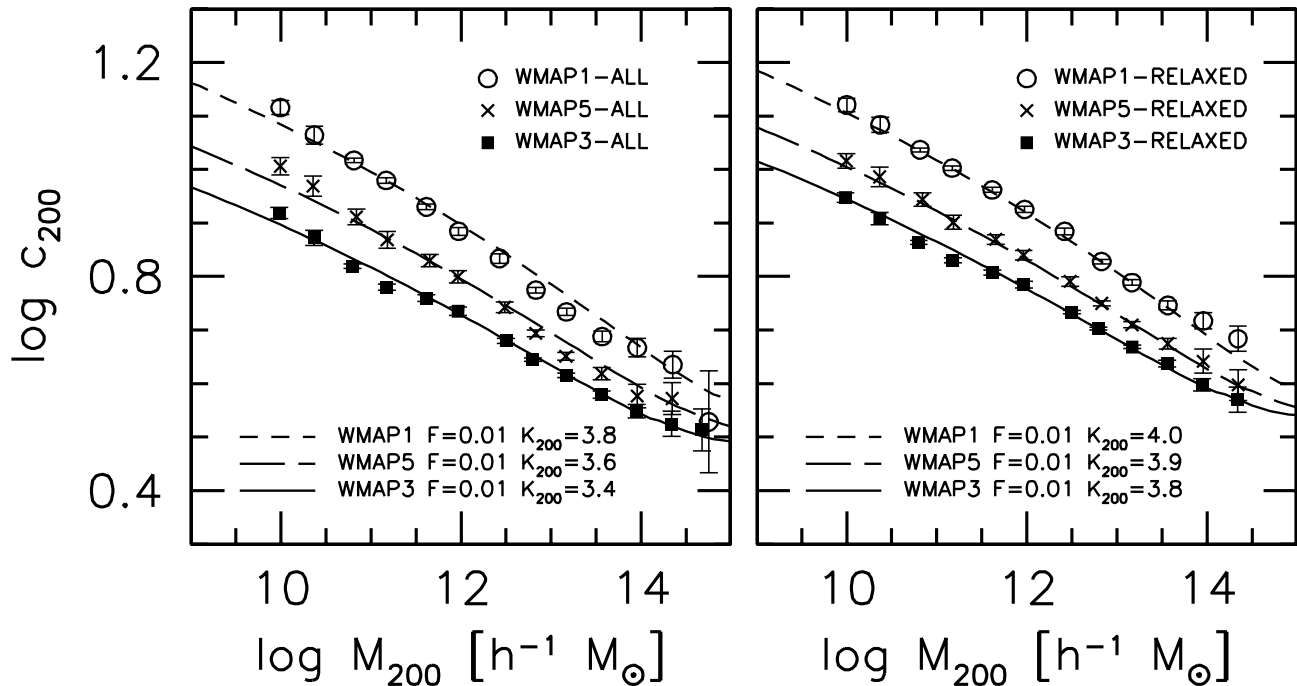


Figure 6. Comparison between the $c_{200} - M_{200}$ relations in our simulations and those predicted by our revised version of the B01 model. Our new model is able to simultaneously fit both the low mass and high mass end of the $c - M$ relation. It provides an excellent fit to the simulations results over more than 4 orders of magnitude in halo mass.

parameter to compare with is the error on the mean (or median) c . Given the numbers in Neto et al. (2007) we obtain a Poisson error of 0.004 dex (i.e. less than 1%) for their lowest mass bin around $10^{12} h^{-1} M_{\odot}$. We obtain similarly small errors with our data for haloes of the same mass. Thus, we argue that despite the large amount of scatter in halo concentrations at fixed halo mass, the discrepancy between the NFW model and the simulation results are very significant: at $M = 10^{12} h^{-1} M_{\odot}$ we find the the NFW model underpredicts the mean concentration by a factor 1.12 (a discrepancy of 0.05 dex in $\log c_{200}$), which increases to a factor of 1.38 (0.14 dex in $\log c_{200}$) at $M = 10^{10} h^{-1} M_{\odot}$. Of course systematic errors in fitting halo concentrations may well be larger than 1%, which would cause them to dominate the error budget. However, the fact that Neto et al. (2007) obtain results that are virtually identical to us using a different N -body simulation code, a different halo finder, and a different fitting procedure, suggests that these effects are not going to mitigate the problem of the NFW model at low masses.

Both the B01 and NFW models predict that the $c - M$ relation is shallower for the WMAP3 cosmology than for the WMAP1 cosmology, in quantitative agreement with the simulation results. However, the problems at high masses for the B01 model and at low masses for the NFW models remain. Another problem for these models is that the normalization of the concentration mass relation in the WMAP3 cosmology is lower than expected based on the parameters K for B01 and C for NFW that are required to match the $c - M$ relation in the WMAP1 cosmology. Since the B01 model does not fit the $c - M$ relation well at high masses, a

straight forward χ^2 minimization gives values of K biased high. Thus, to determine the best-fit values of K , we construct a grid of models with K varying at intervals of 0.1, and chose the value of K which provides the best fit (by eye) over the widest range of halo masses. For $F = 0.01$ the range in mass that is well fitted is $M \sim 10^{10-12} h^{-1} M_{\odot}$, while for $F = 0.001$ the range in mass is $M \sim 10^{11-13} h^{-1} M_{\odot}$.

3.4 A revision of the Bullock model

We now discuss a modification of the B01 model that retains the agreement for galaxy mass haloes, but improves the agreement for group and cluster sized haloes.

Both the B01 and NFW models are based on the idea that the central densities of dark matter haloes reflect the mean density of the universe at a time when the central region of the halo was accreting matter at a high rate. Therefore haloes with central regions that collapse earlier are expected to be denser than haloes that collapse later. Thus the first step in the B01 (and NFW) model is to assign a redshift of collapse, given a halo of mass M_{vir} at a redshift of observation, z .

B01 define the collapse redshift, z_c , as the redshift at which the characteristic mass is equal to a fraction F of the halo mass at the observation redshift, z ,

$$M_*(z_c) = F M_{\text{vir}}(z), \quad (11)$$

Using the spherical collapse formalism, this characteristic mass is defined via

$$\sigma(M_*, z_c) = \sigma(M_*, 0) D(z_c) = 1.686 \quad (12)$$

where $\sigma(M, z)$ is the rms overdensity on mass scale M at redshift z , and $D(z)$ is the linear growth rate.

For comparison, NFW define the collapse redshift as the redshift at which, according to the Press & Schechter formalism (Press & Schechter 1974; Lacey & Cole 1993), half of the virial mass of the halo was first contained in progenitors more massive than a fraction f of the final mass.

The next step in the B01 (and NFW) model is to link the density of the halo at z to that of the mean density of the universe at the collapse redshift. First we define the mass of the halo via

$$M_{\text{vir}}(z) = \frac{4}{3}\pi r_{\text{vir}}^3(z)\Delta_{\text{vir}}(z)\rho_{\text{u}}(z), \quad (13)$$

where Δ_{vir} is the overdensity of the halo relative to the *mean density* of the universe, ρ_{u} . Alternatively one can set $\Delta_{\text{vir}}(z)\rho_{\text{u}}(z) = \Delta(z)\rho_{\text{crit}}(z)$, where Δ is the overdensity of the halo with respect to the *critical density* of the universe, ρ_{crit} . A common choice is to set $\Delta = 200$, which results in the definition of virial mass and radius being independent of cosmology (using units of $h = 1$). Then the characteristic density of the halo at any epoch (as defined by B01) can be written as:

$$\tilde{\rho}_{\text{s}}(z) = \frac{3M_{\text{vir}}(z)}{4\pi r_{\text{s}}^3(z)} = c_{\text{vir}}^3(z)\Delta_{\text{vir}}(z)\rho_{\text{u}}(z), \quad (14)$$

where $c_{\text{vir}}(z) = r_{\text{vir}}(z)/r_{\text{s}}(z)$.

B01 identified the characteristic density of the halo at the observation redshift, z , with the mean density of the universe at the collapse redshift via

$$\tilde{\rho}_{\text{s}}(z) = K^3\Delta_{\text{vir}}(z)\rho_{\text{u}}(z_c) \quad (15)$$

where K is a constant to be determined by calibration against numerical simulations. Since $\rho_{\text{u}}(z_c) = \rho_{\text{u}}(z)(1+z_c)^3/(1+z)^3$, the concentration at the observation redshift is given by

$$c_{\text{vir}}(M_{\text{vir}}, z) = K(1+z_c)/(1+z). \quad (16)$$

Our modification to the B01 model is to simply assume that the characteristic density of the halo $\tilde{\rho}_{\text{s}}$ is independent of redshift (i.e. $\tilde{\rho}_{\text{s}}(z) = \tilde{\rho}_{\text{s}}(z_c)$). Thus

$$c_{\text{vir}}(M_{\text{vir}}, z) = K \left[\frac{\Delta_{\text{vir}}(z_c)\rho_{\text{u}}(z_c)}{\Delta_{\text{vir}}(z)\rho_{\text{u}}(z)} \right]^{1/3} \equiv Kg(z_c, z). \quad (17)$$

As for the original model, the (free) parameter K , which represents the concentration of the halo at the collapse redshift z_c , has to be calibrated against numerical simulations. The function $g(z_c, z)$ specifies the growth of the halo concentration between the redshifts of collapse and observation. Note that this equation is similar to that of the Eke et al. (2001) model, except that they implicitly assumed that $c_{\text{vir}}(z_c) = 1$ (which is wrong), and they define z_c differently.

We can also express g in terms of $\Delta(z)$ and ρ_{crit}

$$g(z_c, z) = \left[\frac{\Delta(z_c)\rho_{\text{crit}}(z_c)}{\Delta(z)\rho_{\text{crit}}(z)} \right]^{1/3} \quad (18)$$

In the case of the $\Delta = 200$ halo definition, we thus have that

$$c_{200}(z) = K_{200} \left[\frac{\rho_{\text{crit}}(z_c)}{\rho_{\text{crit}}(z)} \right]^{1/3} = K_{200} \left[\frac{H(z_c)}{H(z)} \right]^{2/3}. \quad (19)$$

So that the evolution in c_{200} is given by the evolution of the Hubble parameter, which is given by:

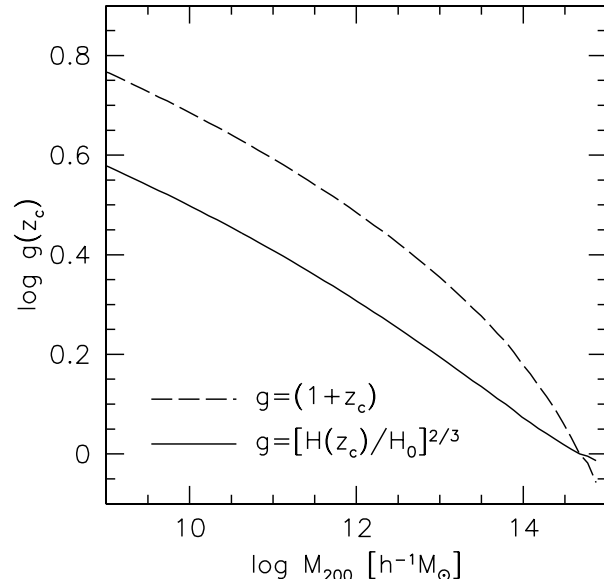


Figure 7. Growth factor of concentration parameter as a function of halo mass (computed at $z = 0$) for WMAP1 cosmology. The dashed line shows the growth factor for the B01 model, while the solid line shows the growth factor for our revised B01 model. Our model has a shallower mass dependence at high masses ($\gtrsim 10^{13}h^{-1}M_{\odot}$), resulting in a better agreement with the high mass end of the concentration mass relation (cf. Fig. 6).

$$\frac{H^2(z)}{H_0^2} = [\Omega_{\Lambda} + \Omega_m(1+z)^3 + (1 - \Omega_{\Lambda} - \Omega_m)(1+z)^2], \quad (20)$$

Our modification of the B01 model only consists of taking account of the redshift dependence of the halo density contrast. In the case of the $\Delta = 200$ halo definition, the redshift dependence of $\Delta_{\text{vir}} = \Delta/\Omega_m$ is completely governed by that of Ω_m . For an EdS universe $\Omega_m(z) = 1$, so that our revised model yields exactly the same $c_{\text{vir}}(z)$ as the original B01 model. However, for a Λ CDM universe Ω_m is a function of redshift, so that the difference between $\Omega_m(z_c)$ and $\Omega_m(z)$ can be significant, and thus also the difference in $c_{\text{vir}}(z)$ between the B01 model and our revised version.

Fig. 7 compares the concentration growth factors, $g(z_c)$ for the B01 model ($g(z_c) = (1 + z_c)$) and for our new model ($g(z_c) = [H(z_c)/H_0]^2/3$) in a WMAP1 cosmology. For haloes below $M = 10^{12}h^{-1}M_{\odot}$ (and collapse redshifts > 2) the slopes of $g(M_{200})$ are the same for both models. This owes to the fact that $\Omega_m(z) \rightarrow 1$ at high redshifts. However for massive haloes (and low collapse redshifts), the concentration growth factor g has a shallower slope in our model than in the original B01 formulation. Because of this difference our new model predicts concentrations at the high mass end that are relatively higher than for the original B01 model. Note also that at the low mass end, the new concentration growth factor is lower than for the B01 model; consequently, in order to match the same c - M relation at the low mass end, the K parameter in our new formulation has to be somewhat higher than in the B01 model.

The symbols in Fig. 6 show the c - M relation obtained from our simulations for all three cosmologies, separately for all haloes (left-hand panel) and for the subsample of relaxed haloes (right-hand panel). The lines correspond to the best-

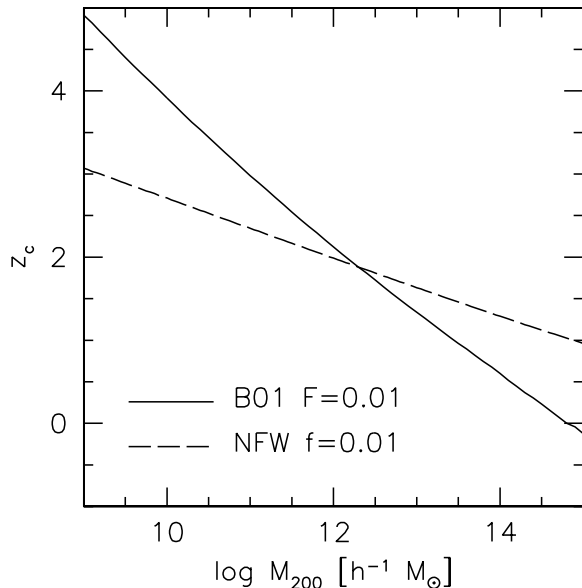


Figure 8. Formation redshifts as a function of halo mass for the B01 and NFW models. The NFW model has a much weaker mass dependence to the formation redshift than the B01 model, which results in a $c - M$ relation much shallower than in the simulations as shown in Figure 5.

fit $c-M$ relations obtained using our new toy model, in which we let K be a free parameter. The best-fit values of K are indicated. Note that our new model can fit the simulation data remarkably well over the entire range of halo masses probed, and for all three cosmologies. Clearly, this new model is a significant improvement over the B01 and NFW models. As with the NFW model and the original B01 model, however, different cosmologies require a different normalization parameter K . In particular, the best-fit value of K decreases going from WMAP1 to WMAP5 to WMAP3. This is unfortunate, as there is currently no existing model that can *a priori* predict the value of K given the cosmology. Consequently, for each cosmology, the best-fit value of K has to be determined empirically using high-resolution numerical simulations. For the three cosmologies considered here, the differences in the best-fit values of K are small ($\simeq 5\%$), but they nevertheless indicate that our model does not fully capture the power spectrum dependence of the $c - M$ relation (nor does the original B01 model. We plan to address this issue in more detail in a future paper.

3.5 Why does the NFW model fail?

There are two differences between the NFW model on the one hand and the B01 model and its modification suggested here on the other: the definition of halo formation redshift, and the method used to link the mean density of the universe at the formation redshift to the concentration of the halo at the observation redshift. Fig. 8 shows the formation redshifts as a function of halo mass for the NFW and B01 models in a WMAP1 cosmology. The NFW model predicts formation redshifts with a significantly shallower mass dependence than the B01 model. We have experimented with a model using the NFW formation time, but the B01 method of linking

formation redshift to halo concentration. For none of these models, however, were we able to obtain a concentration-mass relation with a slope as steep as found in the simulations. Consequently, we conclude that the main problem with the NFW model is its definition of the halo collapse redshift.

3.6 Comparison with observations

Several studies have addressed the issue of the apparent inconsistency between the inner density slopes of dwarf and LSB galaxies and those predicted by CDM (e.g., Moore 1994; Flores & Primack 1994; van den Bosch & Swaters 2001; de Blok et al. 2001, 2002; Swaters et al. 2003, Dutton et al. 2005; Gentile et al. 2005; Simon et al. 2005; Kuzio de Naray et al. 2008). For more massive spiral galaxies the situation is more complicated because the baryons contribute significantly (and may even dominate) the total mass profile in the inner regions, and thus pure CDM predictions are difficult to be tested. For these reasons we limit our comparison to data of dwarf and LSB galaxies. Measuring inner density slopes of dark matter haloes from rotation curves is difficult. A common practice is to fit a power-law to the rotation curve, either to the inner few data points (e.g., de Blok 2001); or to the full rotation curve (e.g. Simon et al. 2005). Both methods have some drawbacks. First of all, the inner few points of the rotation curve carry with them the largest systematic errors. In addition, realistic dark matter halo density profiles (whether they be pseudo-isothermal, NFW, or generalized NFW profiles) all have continuously varying density slopes with radius, so that the results of fitting a single power-law are extremely sensitive to the exact radial range covered. A more robust approach is to fit a double power-law density profile to the entire rotation curve (e.g., van den Bosch & Swaters 2001, Dutton et al. 2005). However, as emphasized by these studies, even in this case there are certain degeneracies inherent to the mass modeling that make it difficult to obtain stringent constraints on the inner density slopes, even with data of high spatial resolution.

In addition to predictions for the slope of the inner density profile, the CDM model also makes predictions regarding the concentration of dark matter haloes. Unfortunately, measuring halo concentrations requires knowledge of the virial radius of the halo, a parameter which is poorly constrained from the observations. This is due to the fact that a rotation curve only probes the inner $\sim 10\%$ of the dark matter halo.

An observationally more robust measurement of the central density is given by the dimensionless parameter $\Delta_{V/2}$, defined as the average density of the halo, with respect to the critical density, inside the radius $R_{V/2}$, where the halo circular velocity drops to half its maximum value (Alam, Bullock & Weinberg 2002).

$$\Delta_{V/2} = \frac{\bar{\rho}(R_{V/2})}{\rho_{\text{crit}}} = 50 \left[\frac{V_{\text{max}}}{\text{km s}^{-1}} \right]^2 \left[\frac{h^{-1} \text{kpc}}{R_{V/2}} \right]^2 \quad (21)$$

For an NFW halo, the circular velocity reaches a maximum, V_{max} , at a radius $r \simeq 2.163 r_s$, so that $R_{V/2} \sim 0.126 r_s$. The maximum circular velocity is given by

$$V_{\text{max}}^2 = 0.2162 V_{\text{vir}}^2 c_{\text{vir}} / f(c_{\text{vir}}), \quad (22)$$

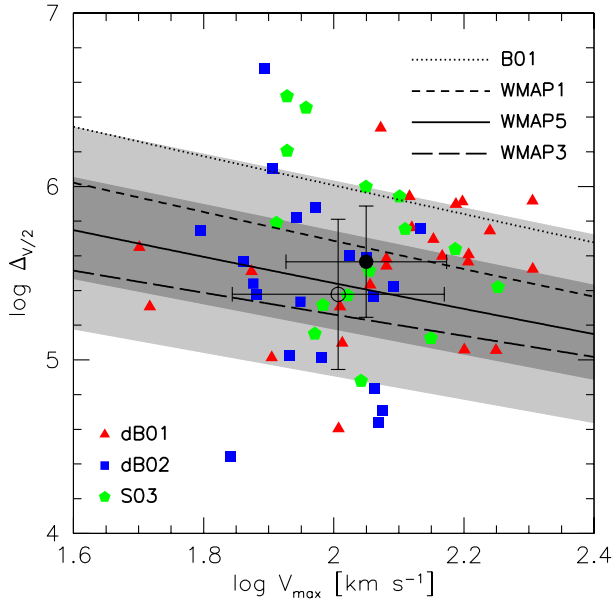


Figure 9. Comparison between the $\Delta_{V/2} - V_{\max}$ relation from observations of dwarf and LSB galaxy rotation curves and the predictions of N-body simulations in a variety of Λ CDM cosmologies. The observations are: de Blok, McGaugh & Rubin (2001, dB01); de Blok & Bosma (2002, dB02); and Swaters et al. (2003, S03). The shaded region shows the 68.3% and 95.4% range of $\Delta_{V/2}$ from our WMAP5 simulations. See text for further details.

where $f(x) = \ln(1+x) - x/(1+x)$. Note that the factor 0.2162 is equal to $f(x)/x$, with $x = 2.163$. The virial velocity scales with the virial mass and virial radius according to

$$\frac{V_{\text{vir}}}{\text{km s}^{-1}} = G^{1/3} \left[\frac{M_{\text{vir}}}{h^{-1} M_{\odot}} \right]^{1/3} \left[\frac{\Delta}{200} \right]^{1/6} \quad (23)$$

$$\frac{V_{\text{vir}}}{\text{km s}^{-1}} = \frac{r_{\text{vir}}}{h^{-1} \text{kpc}} \left[\frac{\Delta}{200} \right]^{1/2} \quad (24)$$

with G the gravitational constant. Using these relations and the definition of the concentration parameter ($c_{\text{vir}} = r_{\text{vir}}/r_s$), $\Delta_{V/2}$ can be expressed purely in terms of the concentration parameter:

$$\Delta_{V/2} = 680.9 \frac{\Delta}{200} \frac{c_{\text{vir}}^3}{f(c_{\text{vir}})}. \quad (25)$$

Thus given a relation between c_{vir} and M_{vir} for NFW haloes, we can convert this into a relation between $\Delta_{V/2}$ and V_{\max} .

Fig. 9 shows the relation between $\Delta_{V/2}$ and V_{\max} for both observations (symbols) and theory (lines). The observations are for dwarf and LSB galaxies, color coded according to the reference. These values are calculated based on the pseudo-isothermal halo fits to the observed rotation curves. We have removed a few galaxies with obviously very bad fits, or for which V_{\max} was poorly constrained by the data. We have verified that including these galaxies makes no significant difference to the median observed $\Delta_{V/2}$. The solid black circle shows the median of the data points, and the error bars reflect the median errors on $\Delta_{V/2}$ and V_{\max} . Although these galaxies are dark matter dominated, the baryons make a

non-negligible contribution to the rotation curve. The open circle shows the median $\Delta_{V/2}$ and V_{\max} for the dark halo when the contribution of the baryons (stars and gas) to the rotation curve has been subtracted. These baryonic contributions are available for about half of the galaxies. This results in a $\Delta_{V/2}$ that is approximately 0.16 dex (i.e., a factor of 1.45) lower, and a V_{\max} that is ~ 0.04 dex (i.e., factor of 1.10) lower. We note that the median $\Delta_{V/2}$ and V_{\max} without subtracting the baryons is the same for this subset, as the full sample, so that the differences in $\Delta_{V/2}$ and V_{\max} are not simply caused by a selection effect.

The lines show the predictions for $\Delta_{V/2} - V_{\max}$ for 4 cosmologies. The dotted line shows the Λ CDM cosmology used in Alam et al. (2002), which has $\Omega_m = 0.3$, $\Omega_{\Lambda} = 0.7$, $\sigma_8 = 1.0$, $h = 0.7$ and $n = 1$. As noted by Alam et al. (2002), this cosmology results in central densities that are a factor of 4 higher than observed. However, this cosmology has values of σ_8 , Ω_m and n that are significantly higher than those for the WMAP cosmologies considered here. The $\Delta_{V/2} - V_{\max}$ relations for WMAP1, WMAP3 and WMAP5 cosmologies are shown as the short dashed, long-dashed and solid lines, respectively. Note that the data are broadly consistent with all these cosmologies; within the errors, the data seem to prefer a cosmology with $\sigma_8 \simeq 0.8$ and $n \simeq 0.96$.

Note, though, that there are several systematic effects that could alter this conclusion. If the effect of halo contraction (e.g. Blumenthal et al. 1986) is taken into account, it will result in a lower $\Delta_{V/2}$ for the initial halo and, and thus favor cosmologies with lower σ_8 . On the other hand, there are several systematic effects that result in underestimates of V_{\max} (see Swaters et al. 2003; Rhee et al. 2004; Hayashi & Navarro 2006; Valenzuela et al. 2007), which will cause the opposite effect and thus would favor cosmologies with higher σ_8 .

For the WMAP5 cosmology we show the 1 and 2- σ dispersion in $\Delta_{V/2}$ assuming a scatter in the $c - M$ relation of $\sigma_{\ln c} = 0.26$ (which results in a scatter of $\simeq 0.28$ dex in $\Delta_{V/2}$). The dispersion of the observed $\Delta_{V/2}$ is $\simeq 0.43$ dex. However, subtracting a measurement uncertainty of 0.32 dex (the median measurement uncertainty from the observations) results in an intrinsic scatter of $\simeq 0.29$ dex, in good agreement with our theoretical predictions.

We conclude therefore, that modulo the caveats of halo contraction and systematic effects (which to first order tend to cancel each other), the central densities of dwarf and LSB galaxies are in good agreement with predictions for a Λ CDM cosmology with parameters favored by the WMAP mission.

However, on larger scales observations seem to require higher concentrations than predicted by Λ CDM. Using X-ray (*Chandra* and *XMM-Newton*) observations of 39 massive galaxy clusters, Buote et al. (2007) obtained $c_{\text{vir}} = 9.0 \pm 0.4$ at $M_{\text{vir}} = 10^{14} M_{\odot}$ for their full sample (covering the mass range $10^{13} \lesssim M_{\text{vir}} \lesssim 10^{15} M_{\odot}$), and $c_{\text{vir}} = 7.6 \pm 0.5$ for the sample restricted to $M_{\text{vir}} \geq 10^{14} M_{\odot}$. Combining strong lensing and X-ray observations, Comerford & Natarajan (2007) found $c_{\text{vir}} = 11.1$ at $M_{\text{vir}} = 10^{14} M_{\odot}$. In our simulations we find the median concentrations of relaxed haloes with $M_{\text{vir}} = 10^{14} M_{\odot}$ to be $c_{\text{vir}} = 6.9$ (WMAP1) and $c_{\text{vir}} = 5.5$ (WMAP3).

The median c_{vir} in the full sample of Buote et al. is a factor 1.30 higher than in our WMAP1 simulations and a factor 1.63 higher than in our WMAP3 simulations. For

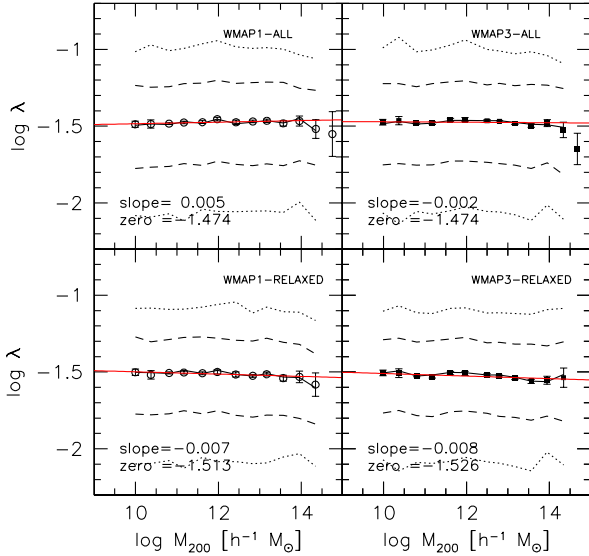


Figure 10. Spin parameter vs. mass for all halos (upper panels) and relaxed halos (lower panels). WMAP5 result are not shown since they do not present any significant difference from WMAP1 or WMAP3. The points represent the median spin in each mass bin, the error bar shows the Poisson error on the mean. The dashed and dotted lines show the 15.9, 84.1, 2.3 and 97.7th percentiles of the distribution. The solid (red) line shows a power-law fit to the $\lambda - M_{200}$ relation: $\log \lambda = \text{zero} + \text{slope}(\log M_{200}/12h^{-1}M_{\odot})$ whose parameters are given in the lower left corner of each panel. Linear fit parameters for the WMAP5 model are reported in Table A1.

the high mass sample of Buote et al. the discrepancies are smaller: a factor of 1.1 for WMAP1 and 1.25 for WMAP3. Given that the scatter in halo concentrations is a factor of 1.3, selection biases in the data (such as selecting the most relaxed clusters, which are likely to form earlier and thus to have higher concentration) could plausibly reconcile the observed concentrations from Buote et al. with the WMAP3 cosmology. The concentrations of Comerford & Natarajan (2007) are a factor 1.6 higher than our WMAP1 results and a factor 2.0 higher than WMAP3 results, and selection effects would have to be rather severe to reconcile even our WMAP1 results with these observations. Another possibility is that halo contraction due to the condensation of baryons at the center of the halo (Blumenthal et al. 1986) has played an important role. However, studies which model the radial density profiles of clusters and elliptical galaxies suggest that it is difficult to reconcile models with adiabatic contraction with observations (Zappacosta et al. 2006; Humphrey et al. 2006, Gastaldello et al. 2007). Thus, it seems that there is a discrepancy between model and data at the high mass end, but not at the low mass end.

This may signal the need for different normalizations of the power spectrum on different scales, which in turn may indicate that the power spectrum has a significant tilt, or a running spectral index with a shallower slope (lower n) at lower masses. However, systematic errors and selection effects in the data need to be understood better before such a conclusion can be verified.

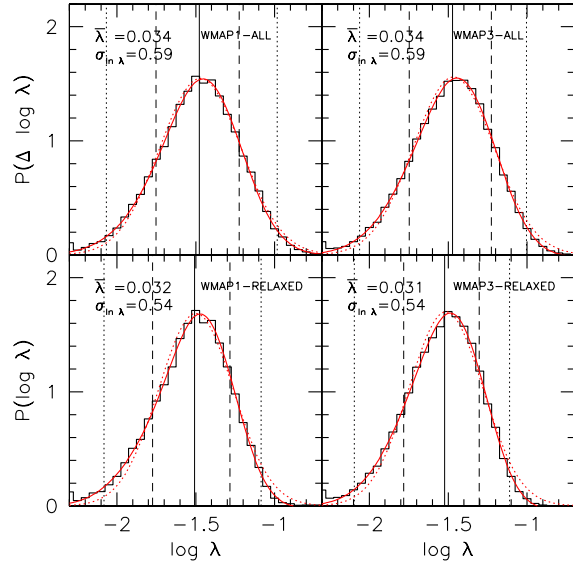


Figure 11. Histograms of the distribution of the halo spin parameters. Only results for WMAP1 and WMAP3 are shown, results for WMAP5 are listed in Table A2. The vertical lines show the 2.3th, 13.9th, 50th, 84.1th, and 97.7th percentiles of the spin residuals. The solid red line shows a Gauss-Hermite polynomial expansion up to fourth order (whose parameters are listed in Table A2), the dashed red line shows the Gaussian corresponding to the zeroth order of this expansion. The mean and the logarithmic variance ($\sigma_{\ln \lambda}$) of the Gaussian fit are reported in the top left corner of each panel.

4 SPIN PARAMETERS

Fig. 10 shows the spin parameter versus halo mass for the WMAP1 (left) and WMAP3 (right) cosmologies for all haloes (top) and for the subsample of relaxed haloes (bottom). As in M07, we find no mass or cosmology dependence of the halo spin parameters. For this reason we do not include the results for the WMAP5 cosmology in the plots. For completeness, we do list the corresponding parameters in Tables A1 and A2 in the Appendix.

Fig. 11 shows the distribution of spin parameters. As with the scatter in concentration, the scatter in λ is not perfectly log-normal. The distribution of spins for all haloes shows a small skewness to low spin parameters. However, we caution against an over interpretation of this skewness, as Bullock et al. (2001b) have demonstrated that haloes with lower spins have larger associated uncertainties, with the error in λ given roughly by $0.2\lambda^{-1}N^{-1/2}$. Thus a halo with 1000 particles will have an uncertainty of 63%, 18%, and 6% for a spin parameter of 0.01, 0.035, and 0.10. Even for haloes with 10000 particles the error on a spin parameter of 0.01 is 20%, which will introduce a non-negligible skewness to the distribution of λ .

We find that the mean, dispersion and skewness of the distributions (see Table A2) are remarkably similar for all three cosmologies considered here, both for the full set of haloes and for the subsample of relaxed haloes. The relaxed haloes have a smaller mean and variance, and a larger skewness. This is due to the removal of un-relaxed haloes which typically have higher spins than relaxed haloes (see M07 for details).

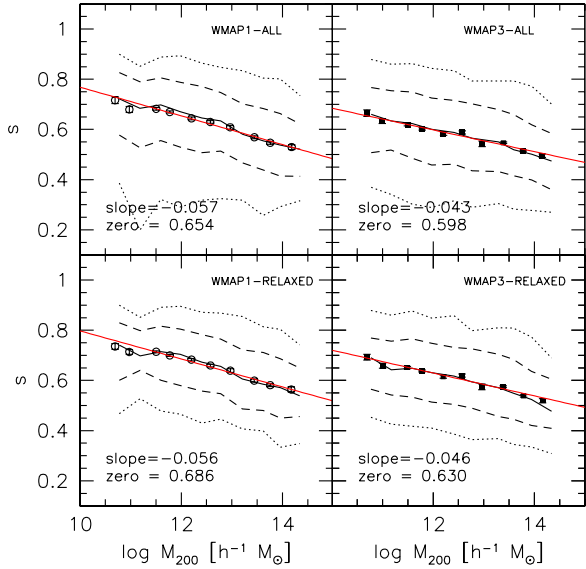


Figure 12. Short to long axis ratio, s , vs mass for WMAP1 (left) and WMAP3 (right), and for all haloes (upper) and relaxed haloes (lower) with $N_{200} > 3000$. WMAP5 model results (not shown) lie in between WMAP1 and WMAP3. The points represent the median value of s spin in each mass bin, the error bar shows the Poisson error on the mean. The dashed and dotted lines show the 15.9, 84.1, 2.3 and 97.7th percentiles of the distribution. The solid (red) line shows a power-law fit to the $s - M_{200}$ relation: $s = \text{zero} + \text{slope}(\log M_{200}/12h^{-1}M_{\odot})$ whose parameters are given in the lower left corner of each panel. Linear fit parameters for the WMAP5 model are reported in Table A1.

5 HALO SHAPES

Fig 12 shows the relation between s (defined as the ratio between the short and long axes) and M_{200} . Here we only consider haloes with at least 3000 particles, because with fewer particles we find evidence for resolution effects. The $s - M_{200}$ relation is well fitted with a power-law of slope $\simeq -0.05$, in all cosmologies and for all and relaxed haloes. Fitting parameters for the shape-mass relation and for its scatter, for all three cosmological models, are listed in Tables A1 and A2 in the Appendix. For the WMAP3 cosmology, the zero point for relaxed haloes is 0.03 higher than for the full sample of haloes. In addition, we find that the zero-point is 0.05 higher for the WMAP1 cosmology compared to that of the WMAP1 cosmology. On the other hand, the relation between p (defined as the ratio between the short and intermediate axes) and M_{200} shows a much weaker correlation, and only a marginal dependence on cosmology (Fig. 13).

Figs. 14 & 15 show the distributions of s and p about the mean relations shown in Figs. 12 & 13. These are roughly Gaussian. The full sample reveals a mild skewness to

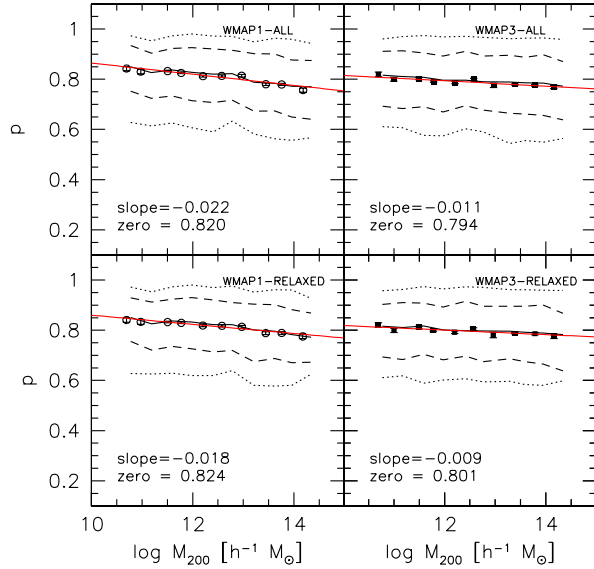


Figure 13. Same of Fig. 12 but for the middle axis, p , vs mass. WMAP5 model results (not shown) lie in between WMAP1 and WMAP3. Values for the *slope* and the *zero* of the linear fit for the WMAP5 model are reported in Table A1.

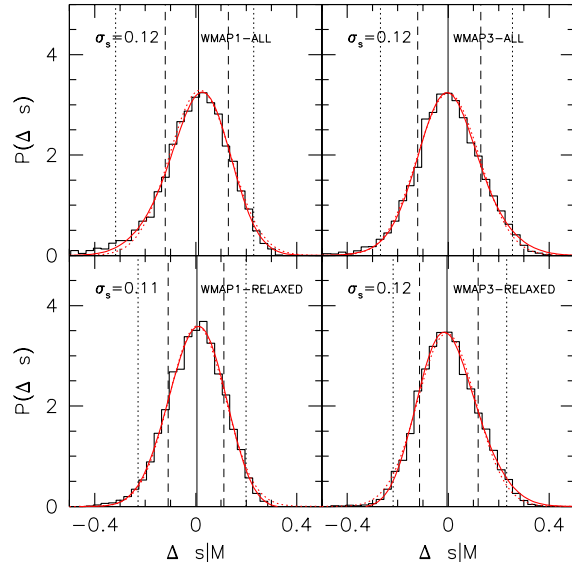


Figure 14. Histograms of scatter in the halo shape parameter s (ratio between minor and major axis length) for WMAP1 (left) and WMAP3 (right); results for WMAP5 (not shown in the plot) are listed in Table A2. The upper panels show all haloes with $N_{200} > 3000$, while the lower panels show the relaxed haloes. The dashed (red) lines show the best fitting Gaussian, while the solid (red) lines show the Gauss-Hermite polynomial expansion (whose parameter are reported in Table A2). The variance of the Gaussian fit is reported in the upper left corner of each panel.

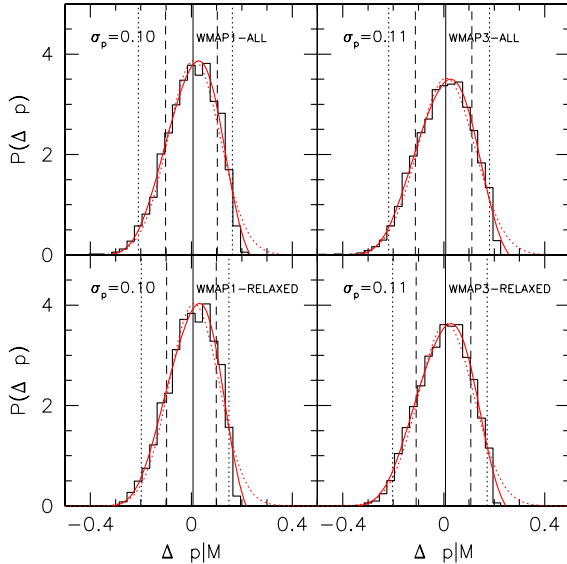


Figure 15. Histograms of scatter in the halo shape parameter p (ratio between minor and intermediate axis length) for WMAP1 (left) and WMAP3 (right); results for WMAP5 (not shown in the plot) are listed in Table A2. The upper panels show all haloes with greater than 3000 particles within r_{200} , while the lower panels show the “relaxed” haloes. The dashed (red) lines show the best fitting Gaussian, while the solid (red) lines show the Gauss-Hermite polynomial expansion (parameters listed in Table A2). The variance of the Gaussian fit is reported in the upper left corner of each panel.

low s , which is most likely due to the presence of unrelaxed haloes.

Allgood et al. (2006) presented a detailed analysis of the dependence of halo shape on mass and on the underlying cosmological model. They found that the redshift, mass and σ_8 dependence of the mean smallest-to-largest axis ratio of haloes is well described by a simple power law relation $\langle s_{0.3} \rangle = a(M_{\text{vir}}/M_*)^b$, where in this case $s_{0.3}$ is measured inside $0.3r_{\text{vir}}$, and the z and σ_8 dependencies are governed by the characteristic non-linear mass, $M_* = M_*(z, \sigma_8)$. Using several simulations they found the following values for the fitting parameters: $a = 0.54 \pm 0.02$ and $b = -0.050 \pm 0.003$.

Fig. 16 shows the mean $s_{0.3}$ -mass and $p_{0.3}$ -mass relations in our simulations. The dotted line shows the relation found by Allgood et al. (2006) where we used the following values for the characteristic mass: $\log(M_*/h^{-1}M_\odot) = 12.82, 12.17$, for the WMAP1 and WMAP3 cosmologies, respectively. Our simulations show a similar slope, but somewhat higher normalization compared to Allgood et al. (2006). In addition, we find that the differences in the shapes between WMAP1 and WMAP3 cosmologies are not simply explained by a difference in M_* , as proposed by Allgood et al. (2006). This can be seen in the upper panels of Fig. 16 by comparing the difference between the Allgood et al. (2006) prediction (dashed line) with the results of our simulations (solid line). This difference is not constant and increases from WMAP1 to WMAP3.

The dot-dashed lines in Fig 16 show s and p within the

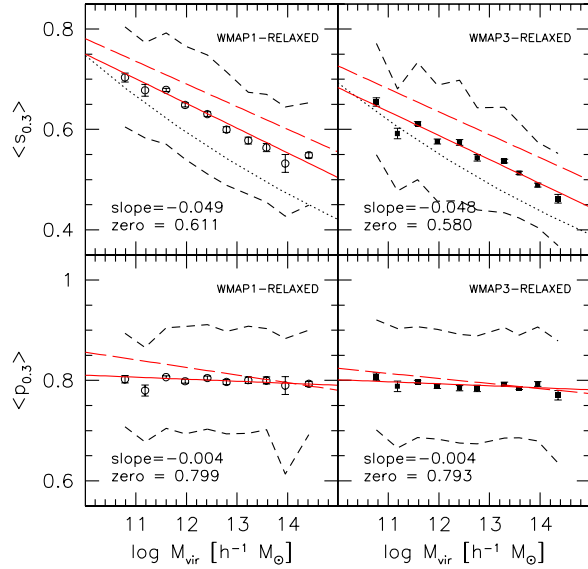


Figure 16. Shape within $0.3r_{\text{vir}}$ versus mass in different cosmological models. A universe with lower σ_8 and Ω_m produces haloes that are more elongated. In the upper panels the dotted lines give the relationship suggested by Allgood et al. (2006). The solid lines show a fit of the form $\text{shape} = \text{zero} + \text{slope}(\log M_{\text{vir}}/M_*)$, where $\log M_* = 12.82, 12.17h^{-1} M_\odot$ in the WMAP1 and WMAP3 cosmologies, respectively. The slopes and zero points of these fits are given in the lower left corner of each panel. The long-dashed lines show the corresponding relations for the shapes measured within the virial radius. The short dashed lines enclose 68.3% of the points, and correspond to a scatter of $\simeq 0.1$.

virial radius. This shows that s decreases towards the center of the halo, in good agreement with Allgood et al. (2006). The dispersion in the axis ratios measured at $0.3r_{\text{vir}}$ is 0.10, only marginally smaller than the dispersions measured within r_{vir} . Results for the shape-mass relation and for the shape distribution for the WMAP5 model (not shown in the figures) are summarized in Table A1 and in Table A2.

6 SUMMARY

In this paper we have used a large set of cosmological N-body simulations in WMAP1, WMAP3 and WMAP5 cosmologies to study how changes in the cosmological parameters affect the halo mass dependence of the concentration parameter, c , the spin parameter, λ , and the halo shape parameters, s and p . The simulations span 5 orders of magnitude in halo mass ($10^{10} - 10^{15} h^{-1} M_\odot$), covering the entire range from haloes those that host individual dwarf galaxies to those associated with massive clusters.

At a fixed mass, haloes in a WMAP3 cosmology are significantly less concentrated than their counterparts in a WMAP1 cosmology. As already noted by other authors this can be ascribed to the lower value for σ_8 in the WMAP3 cosmology compared to WMAP1, that shifts the entire process of structure formation towards lower redshifts. In particular, for a halo of $10^{12} h^{-1} M_\odot$ the WMAP3 concentrations are 1.41 times lower than in a WMAP1 cosmology. Due to this lower normalization, the central densities of dark matter haloes in the WMAP3 cosmology are consistent with the

observed central densities of dark matter haloes of dwarf and LSB galaxies. However, on the scale of clusters, the WMAP3 concentrations may actually be too low compared to observational constraints from X-ray measurements and from gravitational lensing. The WMAP5 concentrations are intermediate between the WMAP1 and WMAP3 cosmologies: they are still consistent with the data on dwarf and LSB galaxies, but somewhat too low on the scale of galaxy clusters. Although this may indicate a problem with the exact shape of the power spectrum of density perturbations, systematic errors and selection effects in the cluster data need to be better understood, before the data can be used to constrain the cosmological spectral index.

We find that for all three cosmologies, the average halo concentration as function of halo mass is well fitted by a single power-law over the entire range of halo masses covered by our simulations. This is *inconsistent* with all existing models for the mass dependence of halo concentrations, which predict that the slope of the c - M relation becomes steeper at higher masses. In particular, the model suggested by Navarro, Frenk, & White (1997) matches the slopes and (to a lesser degree) normalizations of the c - M relation at the massive end ($M \gtrsim 10^{13} h^{-1} M_{\odot}$), but dramatically underpredicts the concentrations for low mass haloes. The model suggested by Bullock et al. (2001a), on the other hand, matches the slopes of the c - M relations for $M \lesssim 10^{13} h^{-1} M_{\odot}$, but underpredicts the concentrations for more massive haloes.

We propose a modification to the B01 model, based on the idea that the characteristic density of a halo remains constant after the halo forms. This results in a growth in halo concentration proportional to $H(z_c)^{2/3}$, rather than $(1+z_c)$ as in the B01 model. Consequently, our new model reproduces the slope of the c - M relation over the full range of masses in our simulations, and for each cosmology. However, as for the original B01 model, the normalization is cosmology dependent (at the level of a few percent), suggesting that the model still does not completely capture the relevant dependencies on the power spectrum. Until such a model is available, the normalization of the c - M relations will have to be calibrated against numerical simulations for each cosmology, if precision concentration parameters are required.

In agreement with previous studies (e.g. Bullock et al. 2001b) we find that the distribution of spin parameters is independent of halo mass and cosmology. There is a trend, though, that less relaxed haloes have higher spin parameters, as previously noticed by Macciò et al. (2007). Finally, we find haloes to be more flattened in the WMAP3 cosmology than in the WMAP1 cosmology, consistent with the suggestion that haloes that form later are more aspherical (Allgood et al. 2006).

ACKNOWLEDGEMENTS

We thank Andrey Kravtsov for helpful discussions, and James Bullock for providing a publically available version of his code which includes our modification (<http://www.physics.uci.edu/~bullock/CVIR/>). The numerical simulations were performed on the zBox2 super-computer at the University of Zürich and on the PIA cluster of the Max-Planck-Institut für Astronomie at the Rechen-

zentrum in Garching. Special thanks to Ben Moore, Doug Potter and Joachim Stadel for bringing zBox2 to life. A.A.D. acknowledges support from the National Science Foundation Grant AST-0507483.

REFERENCES

- Alam S. M. K., Bullock J. S., Weinberg D. H. 2002, ApJ, 572, 34
- Allgood B., Flores R. A., Primack J. R., Kravtsov A. V., Wechsler R. H., Faltenbacher A., Bullock J. S. 2006, MNRAS, 367, 1781
- Bertschinger E. 2001, ApJS, 137, 1
- Blumenthal G. R., Faber S. M., Flores R., Primack J. R. 1986, ApJ, 301, 27
- Bullock J. S., Kolatt T. S., Sigad Y., Somerville R. S., Kravtsov A. V., Klypin A. A., Primack J. R., Dekel A. 2001a, MNRAS, 321, 559 (B01)
- Bullock J. S., Dekel A., Kolatt T. S., Kravtsov A. V., Klypin A. A., Porciani C., Primack J. R. 2001b, ApJ, 555, 240
- Buote D. A., Gastaldello F., Humphrey P. J., Zappacosta L., Bullock J. S., Brighenti F., Mathews W. G. 2007, ApJ, 664, 123
- Comerford J. M., Natarajan P. 2007, MNRAS, 379, 190
- de Blok W. J. G., McGaugh S. S., Rubin V. C. 2001, AJ, 122, 2396
- de Blok W. J. G., Bosma A. 2002, A&A, 385, 816
- Duffy A., Schaye J., Kay S., Dalla Vecchia C. 2008, arXiv:0804.2486, MNRAS in press
- Dutton A. A., Courteau S., de Jong R., Carignan C. 2005, ApJ, 619, 218
- Dutton A. A., van den Bosch F. C., Dekel A., Courteau S. 2007, ApJ, 654, 27
- Eke V. R., Navarro J. F., Steinmetz M. 2001, ApJ, 554, 114
- Flores R. A., Primack J. R. 1994, ApJL, 427, L1
- Gastaldello, F., Buote, D. A., Humphrey, P. J., Zappacosta, L., Bullock, J. S., Brighenti, F., & Mathews, W. G. 2007, ApJ, 669, 158
- Gentile, G., Burkert, A., Salucci, P., Klein, U., & Walter, F. 2005, ApJL, 634, L145
- Hayashi E., Navarro J. F. 2006, MNRAS, 373, 1117
- Humphrey P. J., Buote D. A., Gastaldello F., Zappacosta L., Bullock J. S., Brighenti F., Mathews W. G. 2006, ApJ, 646, 899
- Jing Y. P., Suto Y. 2002, ApJ, 574, 538
- Komatsu E., et al. 2008, ArXiv e-prints, 803, arXiv:0803.0547
- Kuzio de Naray R., McGaugh S. S., de Blok W. J. G. 2008, ApJ, 676, 920
- Kuhlen M., Strigari L. E., Zentner A. R., Bullock J. S., Primack J. R. 2005, MNRAS, 357, 387
- Lacey C., Cole S. 1993, MNRAS, 262, 627
- Li Y., Mo H.J., van den Bosch F.C., Lin W.P., 2007, MNRAS, 379, 689
- Macciò A. V., Murante G., Bonometto S. A. 2003, ApJ, 588, 35
- Macciò A. V., Dutton A. A., van den Bosch F. C., Moore B., Potter D., Stadel J. 2007, MNRAS, 378, 55 (M07)

- Mainini R., Macciò A. V., Bonometto S. A., Klypin A. 2003, *ApJ*, 599, 24
- Mo H. J., Mao S., White S. D. M. 1998, *MNRAS*, 295, 319
- Moore B. 1994, *Nature*, 370, 629
- Navarro J. F., Frenk C. S., White S. D. M. 1996, *ApJ*, 462, 563
- Navarro J. F., Frenk C. S., White S. D. M. 1997, *ApJ*, 490, 493 (NFW)
- Neto A. F., et al. 2007, *MNRAS*, 381, 1450
- Press W. H., Schechter P. 1974, *ApJ*, 187, 425
- Rhee G., Valenzuela O., Klypin A., Holtzman J., Moorthy B., 2004, *ApJ*, 617, 1059
- Shaw L. D., Weller J., Ostriker J. P., Bode P. 2006, *ApJ*, 646, 815
- Sheth R. K., Tormen G. 2002, *MNRAS*, 329, 61
- Simon J. D., Bolatto A. D., Leroy A., Blitz L., Gates E. L. 2005, *ApJ*, 621, 757
- Spergel D. N., et al. 2003, *ApJS*, 148, 175
- Spergel D. N., et al. 2007, *ApJS*, 170, 377
- Springel V., et al. 2005, *Nature*, 435, 629
- Stadel J. G. 2001, Ph.D. Thesis, University of Washington
- Swaters R. A., Madore B. F., van den Bosch F. C., Balcells M., 2003, *ApJ*, 583, 732
- Valenzuela O., Rhee G., Klypin A., Governato F., Stinson G., Quinn T., Wadsley J., 2007, *ApJ*, 657, 773
- van den Bosch F.C., 2002, *MNRAS*, 331, 98
- van den Bosch F. C., Swaters R. A. 2001, *MNRAS*, 325, 1017
- Wechsler R.H., Bullock J.S., Preimack J.R., Kravtsov A.V., Dekel A., 2002, *ApJ*, 568, 52
- Zappacosta L., Buote D. A., Gastaldello F., Humphrey P. J., Bullock J., Brighenti F., Mathews W. 2006, *ApJ*, 650, 777
- Zentner A. R., Bullock J. S. 2002, *Phy.Rev.D*, 66, 043003
- Zhao D. H., Mo H. J., Jing Y. P., Börner, G. 2003a, *MNRAS*, 339, 12
- Zhao D.H., Jing Y.P., Mo H.J., Börner G., 2003b, *ApJ*, 597, 9

APPENDIX A: PARAMETERS

In the appendix we summarize all the parameters of the fitting functions used through this paper. Table A1 contains the slope, zero and relative errors for the power-laws fits shown in Figs. 2, 3, 10, 12. Table A2 shows the parameters describing the distribution around the mean of concentrations, spin and shapes in the three different cosmological models (Figs: 4, 11, 14, 15). While this paper was ready for submission a similar study of the concentration mass-relation for the WMAP5 cosmology was presented in Duffy et al. (2008). They limited their studied only to haloes defined with more than 10^4 particles inside the virial radius. This left them with only 1269 haloes, nevertheless the slope of their power law fit is consistent with our results (within the errors) for both the ALL and RELAXED sample.

Table A1. Parameters of the power-law fits shown in Figs.2, 3, 10, 12, & 13. The data are fitted with the power law $y = \text{zero} + \text{slope}(\log M - 12)$, where M is in units of $h^{-1} M_{\odot}$. The second column reports the mass range over which the fit has been obtained, the third the number of haloes within this mass range (using all the simulations listed in Table 2).

sample	N_{min}	$\log_{10} M$ [$h^{-1} M_{\odot}$]	N_{haloes}	zero	error	slope	error
<i>log c_{vir} vs log M_{vir}</i>							
W1-ALL	500	9.83-14.95	29693	1.011	0.001	-0.114	0.001
W1-RELAXED	500	9.83-14.95	21876	1.051	0.001	-0.099	0.001
W3-ALL	500	9.82-14.95	49830	0.861	0.001	-0.086	0.001
W3-RELAXED	500	9.82-14.95	33913	0.915	0.001	-0.080	0.001
W5-ALL	500	9.84-14.86	12184	0.925	0.001	-0.108	0.001
W5-RELAXED	500	9.84-14.86	8282	0.971	0.001	-0.094	0.001
<i>log c_{200} vs log M_{200}</i>							
W1-ALL	500	9.83-14.92	25952	0.879	0.001	-0.119	0.001
W1-RELAXED	500	9.83-14.85	19528	0.917	0.001	-0.104	0.001
W3-ALL	500	9.82-14.82	40027	0.719	0.001	-0.088	0.001
W3-RELAXED	500	9.82-14.82	28344	0.769	0.001	-0.083	0.001
W5-ALL	500	9.84-14.93	9988	0.787	0.001	-0.110	0.001
W5-RELAXED	500	9.84-14.93	7060	0.830	0.001	-0.098	0.001
<i>log λ vs log M_{200}</i>							
W1-ALL	500	9.83-14.92	25733	-1.474	0.002	0.005	0.002
W1-RELAXED	500	9.83-14.92	19377	-1.513	0.002	-0.007	0.002
W3-ALL	500	9.82-14.82	39662	-1.474	0.001	-0.002	0.001
W3-RELAXED	500	9.82-14.82	28114	-1.526	0.001	-0.008	0.001
W5-ALL	500	9.84-14.93	9988	-1.458	0.004	0.001	0.003
W5-RELAXED	500	9.84-14.93	7060	-1.505	0.004	-0.009	0.004
<i>s vs log M_{200}</i>							
W1-ALL	3000	10.61-14.92	4886	0.654	0.015	-0.057	0.016
W1-RELAXED	3000	10.61-14.85	3820	0.686	0.017	-0.056	0.018
W3-ALL	3000	10.60-14.82	6022	0.598	0.016	-0.043	0.013
W3-RELAXED	3000	10.60-14.82	4273	0.630	0.018	-0.046	0.016
W5-ALL	3000	10.60-14.82	1492	0.623	0.035	-0.052	0.025
W5-RELAXED	3000	10.61-14.93	1060	0.657	0.040	-0.054	0.029
<i>p vs log M_{200}</i>							
W1-ALL	3000	10.61-14.92	4886	0.820	0.015	-0.022	0.016
W1-RELAXED	3000	10.61-14.85	3820	0.824	0.017	-0.018	0.018
W3-ALL	3000	10.60-14.82	6022	0.794	0.016	-0.011	0.013
W3-RELAXED	3000	10.60-14.82	4273	0.801	0.018	-0.009	0.016
W5-ALL	3000	10.60-14.82	1492	0.807	0.035	-0.016	0.025
W5-RELAXED	3000	10.61-14.93	1060	0.812	0.040	-0.014	0.029

Table A2. Parameters of the distribution of concentrations (Fig 4), spin (Fig. 11), and shapes (Figs. 14 & 15). The distribution have been fitted by a Gauss-Hermite polynomial expansion up to fourth order ($h_1 - h_4$). The zeroth order of this expansion is a Gaussian fit, whose mean $\langle \Delta \log c \rangle$ and dispersion $\sigma_{\Delta \log c}$ are determined by setting $h_1 = h_2 = 0$. Columns 6-10 show the 2.3, 15.9, 50.0, 84.1, and 97.7th percentiles of the distribution.

sample	$\langle \Delta \log c \rangle$	$\sigma_{\Delta \log c}$	h_3	h_4	2.3th	15.9th	50th	84.1th	97.7th
$\Delta \log c_{200} M_{200}$									
W1-ALL	0.033	0.129	-0.670	0.356	-0.405	-0.143	0.022	0.146	0.269
W1-RELAXED	0.011	0.111	-0.421	0.216	-0.263	-0.113	0.007	0.115	0.228
W3-ALL	0.040	0.132	-0.880	0.252	-0.417	-0.147	0.027	0.150	0.252
W3-RELAXED	0.015	0.109	-0.622	0.146	-0.260	-0.113	0.010	0.114	0.209
W5-ALL	0.041	0.130	-0.929	0.351	-0.417	-0.148	0.028	0.149	0.252
W5-RELAXED	0.015	0.105	-0.620	0.259	-0.268	-0.110	0.011	0.112	0.209
$\log \lambda$									
W1-ALL	-1.470	0.258	-0.158	0.050	-2.069	-1.752	-1.478	-1.225	-0.984
W1-RELAXED	-1.499	0.236	-0.307	0.034	-2.083	-1.774	-1.508	-1.284	-1.085
W3-ALL	-1.465	0.256	-0.194	-0.003	-2.062	-1.747	-1.472	-1.227	-1.004
W3-RELAXED	-1.514	0.235	-0.297	-0.019	-2.095	-1.783	-1.522	-1.303	-1.110
W5-ALL	-1.466	0.253	-0.162	0.051	-2.070	-1.743	-1.468	-1.218	-0.942
W5-RELAXED	-1.508	0.228	-0.341	0.041	-2.105	-1.774	-1.515	-1.297	-1.065
$\Delta s M_{200}$									
W1-ALL	0.017	0.121	-0.343	0.098	-0.317	-0.121	0.011	0.130	0.230
W1-RELAXED	0.004	0.112	-0.123	-0.123	-0.224	-0.110	0.003	0.112	0.205
W3-ALL	0.007	0.123	0.215	0.169	-0.269	-0.121	-0.001	0.129	0.255
W3-RELAXED	-0.006	0.116	0.441	0.011	-0.218	-0.113	-0.004	0.119	0.232
W5-ALL	0.008	0.128	-0.117	0.196	-0.294	-0.129	0.004	0.133	0.248
W5-RELAXED	-0.002	0.117	0.321	-0.031	-0.233	-0.114	-0.003	0.123	0.221
$\Delta p M_{200}$									
W1-ALL	0.011	0.103	-0.779	-0.514	-0.209	-0.102	0.006	0.103	0.162
W1-RELAXED	0.011	0.100	-0.867	-0.504	-0.203	-0.099	0.005	0.100	0.155
W3-ALL	0.010	0.113	-0.596	-0.491	-0.218	-0.113	0.008	0.112	0.181
W3-RELAXED	0.010	0.110	-0.731	-0.525	-0.203	-0.109	0.007	0.108	0.173
W5-ALL	0.009	0.109	-0.477	-0.335	-0.218	-0.109	0.004	0.106	0.185
W5-RELAXED	0.006	0.103	-0.451	-0.287	-0.198	-0.101	0.005	0.100	0.178